Granular Aluminum Parametric Amplifier for Low-Noise Measurements in Tesla Fields

Nicolas Zapata,[1,*] Ivan Takmakov,[1,2,†] Simon Günzler,[1,2] Simon Geisert,[1] Soeren Ihssen,[1] Mitchell Field,[1]
Ameya Nambisan,[1] Dennis Rieger,[2] Thomas Reisinger,[1] Wolfgang Wernsdorfer,[1,2] and Ioan M. Pop[1,2,3,‡]

[1]*IQMT, Karlsruhe Institute of Technology, 76131 Karlsruhe, Germany*
[2]*PHI, Karlsruhe Institute of Technology, 76131 Karlsruhe, Germany*
[3]*Physics Institute 1, Stuttgart University, 70569 Stuttgart, Germany*

Josephson junction parametric amplifiers have become essential tools for microwave quantum circuit readout with minimal added noise. Even after improving at an impressive rate in the past decade, they remain vulnerable to magnetic fields, which limits their use in many applications such as spin qubits, Andreev and molecular magnet devices, dark matter searches, etc. Kinetic inductance materials, such as granular aluminum (grAl), offer an alternative source of nonlinearity with innate magnetic field resilience. We present a nondegenerate amplifier made of two coupled grAl resonators resilient to in-plane magnetic fields up to 1T. It offers 20 dB of gain close to the quantum limit of added noise, with a gain-bandwidth product of 28 MHz and −110 dBm input saturation power.

The remarkable progress in Josephson junction (JJ) based parametric amplifiers sparked their adoption in both academic and industrial research groups, establishing single-shot quantum state detection of superconducting qubits as an integral capability in circuit quantum electrodynamics [1–4]. State-of-the-art amplifiers are essential for syndrome measurements during error correction of superconducting quantum registers [5–8], they enable the development of novel detection techniques [9–13], and serve as indispensable instruments to uncover microscopic mechanisms degrading superconducting qubit coherence [14–16]. However, the magnetic-field-induced Fraunhofer pattern for the JJ critical current [17–19] constrains their applicability in systems such as spin [12,20,21] and Andreev qubits [22,23], spin ensembles [24,25], molecular magnet devices [26], and dark matter detectors [27–29].

Recent experiments have used magnetic shielding to protect JJ-based amplifiers [12,21,30], at the price of placing the amplifier farther from the measured device and risking to reduce the readout efficiency. Ideally, a magnetic field resilient amplifier is directly coupled to the device under test. Graphene-based amplifiers [31,32] and devices employing proximitized semiconductors [33,34] have been developed to achieve this goal. However, technologically involved fabrication makes their integration into more complex systems challenging, and their relatively low saturation power (−130 to −120 dBm) limits the readout signal amplitude. An alternative path employs the nonlinearity of kinetic inductance materials like NbN [35,36], NbTiN [37–40], or granular aluminum (grAl) [41,42], which offer magnetic field resilience, adaptable integration, and larger dynamic range.

Remarkable progress has recently been reported for NbN amplifiers, which were proven to operate close to the quantum limit up to 0.5 T [35]. Even though NbN enabled these achievements, its relatively large critical current density, in the range of $\mathrm{mA}/\mu\mathrm{m}^2$, requires pushing the boundaries of device miniaturization to reach nonlinearity values comparable to JJ devices. Two orders of magnitude lower critical current densities and higher nonlinearity can be achieved in grAl [41–43] while remaining an order of magnitude below the superconducting-to-insulator transition threshold [44–47].

In this Letter, we tailor the nonlinearity of grAl to fabricate a standing wave parametric amplifier (grAlPA), which operates near the quantum limit in magnetic fields up to 1 T in plane. We obtain 20 dB amplification, 28 MHz gain-bandwidth product, and a saturation power of −110 dBm, satisfying typical requirements for quantum device readout. These features make grAlPAs convenient and powerful tools, ready to be integrated and to extend the range of quantum limited readout applications.

The grAlPA amplifier, operated in reflection, consists of two capacitively coupled grAl resonators mounted in a single-port cylindrical waveguide, coupled via evanescent electric field to a coaxial cable [cf. Figs. 1(a) and 1(b)]. The resonators are formed by two coplanar capacitor plates connected by a central grAl strip [cf. Figs. 1(c) and 1(d)] which gives 80% of the total inductance [48]. The dimensions of the capacitor plates are chosen to match the

[*]Contact author: nicolas.gonzalez2@kit.edu
[†]Present address: IQM Quantum Computers, Espoo 02150, Finland.
[‡]Contact author: ioan.pop@kit.edu

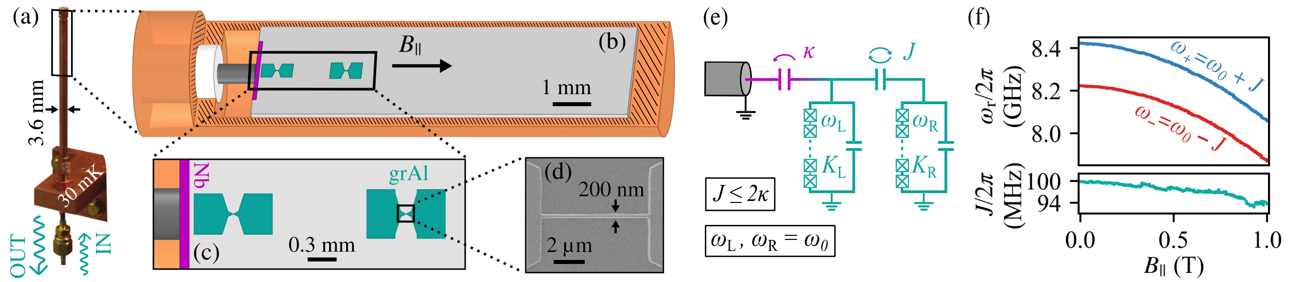

FIG. 1. Device design and frequency dependence in magnetic fields up to 1 T. (a),(b) Photograph and schematics of the sample holder used for microwave reflection measurements, similar to Refs. [42,62,63]. (c) The granular aluminum parametric amplifier (grAlPA) consists of a pair of lumped-element grAl resonators (green), comprised of two coplanar capacitor plates connected by a central strip. To stabilize the evanescent field coupling of the grAlPA to the coaxial central pin (black), we add a Nb pad (purple) at the edge of the substrate [48]. (d) Scanning electron beam image of the central grAl nanostrip. (e) Equivalent circuit diagram of the grAlPA. The design resembles a Bose-Hubbard dimer, similar to Refs. [64,65]. The grAl strip shown in (c) can be modeled as an array of Josephson junctions [41,66] with a self-Kerr nonlinearity denoted as K_i ($i = R, L$). The hopping interaction J gives rise to a pair of hybridized modes $\omega_\pm$. (f) Measured frequency dependence of the dimer $\omega_\pm$ (top) and hopping interaction J (bottom) as a function of in-plane magnetic fields up to 1 T.

frequencies of the two modes and target perfect hybridization. The device is fabricated in a single-step electron beam lithography, followed by zero-angle evaporation on a c-plane sapphire substrate [48]. We deposit an 830 μΩ cm resistivity grAl film, 40 nm thick, which gives 120 pH/□ of kinetic inductance.

The waveguide provides a clean microwave environment for the grAlPA thanks to its ≈60 GHz cutoff frequency, a factor of 5 above its operational range. The challenge when using this strategy arises from the exponential susceptibility of the coupling to variations in the distance between the pin and the grAlPA. In order to mitigate this effect, we add a 40-μm-wide and 40-nm-thick Nb pad at the edge of the chip using optical lithography. The Nb coupling pad acts as an on-chip extension of the coaxial cable central pin, uniformly spreading the electric field lines toward the grAlPA [48].

Figure 1(e) shows the equivalent grAlPA circuit, which can be modeled by the following Bose-Hubbard-dimer Hamiltonian [64,65,67]:

$$H/\hbar = \sum_{i=\mathrm{L,R}} \left(\omega_i a_i^\dagger a_i + \frac{K_i}{2} a_i^\dagger a_i^\dagger a_i a_i \right) + J a_\mathrm{L}^\dagger a_\mathrm{R} + \mathrm{H.c.}, \quad (1)$$

where the two bosonic modes a_i, with $i = \mathrm{L, R}$, correspond to the left and right grAl resonators, respectively. The individual resonant frequencies are ω_i, the on-site potentials K_i are given by the first-order Kerr nonlinearity of the central grAl strips, and the hopping term J arises from the electric dipole-dipole interaction between the resonators. In the case of perfect hybridization $\omega_\mathrm{L} = \omega_\mathrm{R} = \omega_0$, this interaction leads to the formation of the hybridized dimer modes $\omega_\pm = \omega_0 \pm J$, each sharing the total coupling κ of the left resonator to the microwave environment [48]. When a pump is applied between the hybridized modes, four-wave mixing converts two pump photons into one signal and one idler photon in the two dimer modes, respectively, implementing a phase-preserving amplifier with signal-pump detuning J.

While Eq. (1) has the necessary ingredients for parametric amplification, in order to achieve a practically useful device, two conditions need to be fulfilled. First, the Kerr coefficients $K_i/2\pi$ should be ≈1–100 kHz, as higher values reduce the amplifier compression point below the power commonly needed for device readout (≈ -140 dBm) [68,69] and subkilohertz coefficients require higher pump powers for 20 dB gain performance, which increase the heat load on the cryostat [70]. By using a grAl strip 0.2 μm wide and 7 μm long, we obtain $K_i/2\pi = 2 \pm 1$ kHz [48]. Second, for both modes to be efficiently driven by the same pump, the coupling strength should satisfy the condition $J \lesssim 2\kappa$ [66]. At the same time, to maximize the gain-bandwidth product, we aim to increase κ as much as possible. We design the grAlPA to have $J/2\pi = 0.1$ GHz and $\kappa/2\pi = 60$ MHz.

When exposed to an in-plane magnetic field, the dimer shifts down in frequency as shown in the upper panel in Fig. 1(f), tuning by approximately 300 MHz at $B_{||} = 1$ T, without suffering from added losses [48]. This shift is explained by an increase of the grAl kinetic inductance, corresponding to a suppression of the superconducting gap (cf. Refs. [42,43,48,62]). We mechanically align the field to within 1% in plane, and we compensate *in situ* the remaining out-of-plane component using a custom-designed 2D vector magnet [48]. Importantly, the hopping strength J changes by less than 10% over the entire field range, preserving the conditions for parametric amplification up to 1 T [cf. lower panel in Fig. 1(f)].

Figure 2(a) shows the gain performance of the grAlPA in zero magnetic field, as a function of increasing pump power at fixed frequency. We define the gain of the amplifier as the ratio between the reflected power with the pump on and off.

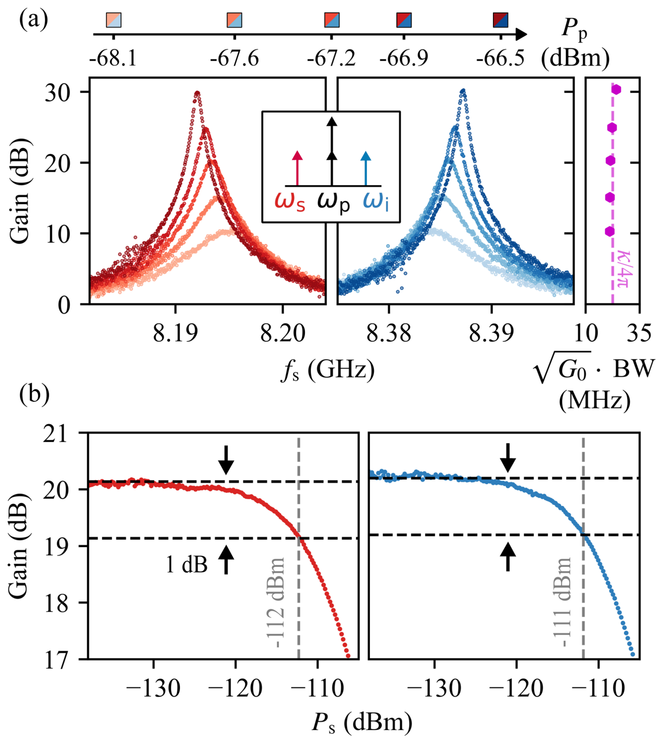

FIG. 2. Gain performance in zero field. (a) grAlPA gain vs signal frequency f_s, for different pump powers P_p and fixed pump frequency $f_p = 8.29$ GHz. The inset shows a schematic of the four-wave mixing process: two pump photons (black line) are converted into a signal photon (red line) and an idler photon (blue line), each populating a dimer mode. The right-hand panel shows the measured gain-bandwidth product. (b) Saturation power measurements for the grAlPA modes. P_s is the input signal power, and the gray labels indicate the corresponding to 1-dB compression point.

Note that, by this choice, possible internal losses produce asymmetric gain profiles. By increasing the pump power, we can obtain a maximum gain G_0 of 30 dB before entering the multistable regime [48]. We measure a constant gain-bandwidth product $\sqrt{G_0} \cdot \mathrm{BW} = (\kappa/2)/2\pi = 22.5$ MHz, as illustrated in the right-hand panel in Fig. 2(a). Conveniently, the signal-pump detuning is in the 0.1 GHz range, as expected from the design value for the hopping term J, facilitating pump tone filtering at the output of the grAlPA.

The dynamic range of the grAlPA is quantified by the input signal-probe power for which the maximum gain G_0 decreases by 1 dB, i.e., the 1-dB compression point. For this purpose, we calibrate the attenuation of the input line using the resonance fluorescence of a frequency-tunable transmon qubit [71,72] in a separate experiment, employing the same setup and sample holder utilized for the grAlPA. We sample several frequencies in the interval of interest and interpolate in between, thereby calibrating the line attenuation in a 1.5 GHz frequency range [48]. As presented in Fig. 2(b), for $G_0 = 20$ dB, we obtain 1-dB compression points of -111 ± 2 dBm in both modes. This dynamic range is on par with previous implementations using arrays of Josephson junctions [65,69,73,74] and can be improved by increasing the coupling κ to match state-of-the-art devices [6,75].

In Fig. 3(a), we demonstrate that the grAlPA can be successfully operated at $G_0 = 20$ dB gain in magnetic fields up to 1 T. Because of the field dependence of the dimer frequency, at each field bias, the frequency of the pump needs to be adjusted, as indicated by the arrows in Fig. 3(a). The measured 30% decrease of $\sqrt{G_0} \cdot \mathrm{BW}$ from zero field to 1 T shown in Fig. 3(a) is explained by the progressive decoupling of the dimer as the modes move away from the cylindrical waveguide cutoff [48]. In Figs. 3(b) and 3(c), we present measured 20 dB gain profiles in $B_\parallel = 1$ T and their corresponding power saturation. We find it remarkable that the grAlPA performance at $B_\parallel = 1$ T is comparable to that at $B_\parallel = 0$ T. The shoulder visible in the line shape of the high-frequency mode is explained by a 1-dB dip in the background signal measured without the pump, due to internal losses in the grAl resonators [48].

Arguably the most important figure of merit of parametric amplifiers is the improvement they provide to the signal-to-noise ratio (SNR) of a readout chain. In Fig. 4(a), we illustrate the near-quantum limited noise performance of the grAlPA at 0 T. We measure the power spectral density (PSD) of the output line connected to the grAlPA, with the pump on and off. We convert the PSD to temperature scale, using a power-calibrated pilot tone at $f_s = 8.193$ GHz [48]. When the pump is off, the $\approx$4 K noise floor is set by a high electron mobility transistor (HEMT). By operating the grAlPA at 20 dB gain, we obtain 10 dB of SNR improvement (ΔSNR), corresponding to an input-referred noise close to the standard quantum limit for phase-preserving amplifiers [76].

The grAlPA noise performance under in-plane magnetic fields up to $B_\parallel = 1$ T is shown in Fig. 4(b). For each point, we fix the gain of the amplifier to $G_0 = 20$ dB and tune the power-calibrated pilot tone to match the shift of the gain profiles in field [cf. Fig. 3(a)]. We report the input referred noise n_{in} in units of photons, calculated using the relation $n_{\mathrm{in}} = k_B \bar{T}_{\mathrm{in}}/h f_s$, where $\bar{T}_{\mathrm{in}}$ is the noise temperature floor extracted from the PSD with the grAlPA on. The quantum limit is given by $n_{\mathrm{in}} = 1$, where half a photon is added by the amplifier and half a photon originates from input vacuum fluctuations. In zero field, we obtain $n_{\mathrm{in}} = 1.21 \pm 0.63$, corresponding to an effective grAlPA added noise $n_{\mathrm{gr}} = 0.71 \pm 0.63$. Remarkably, the grAlPA remains near quantum limited up to $B_\parallel = 1$ T, illustrating its utility for quantum readout in magnetic field. We attribute the upturn visible in the grAlPA noise above 0.6 T to spurious vortices in the capacitor pads, which can create additional loss channels [77,78] and should be suppressed in future designs.

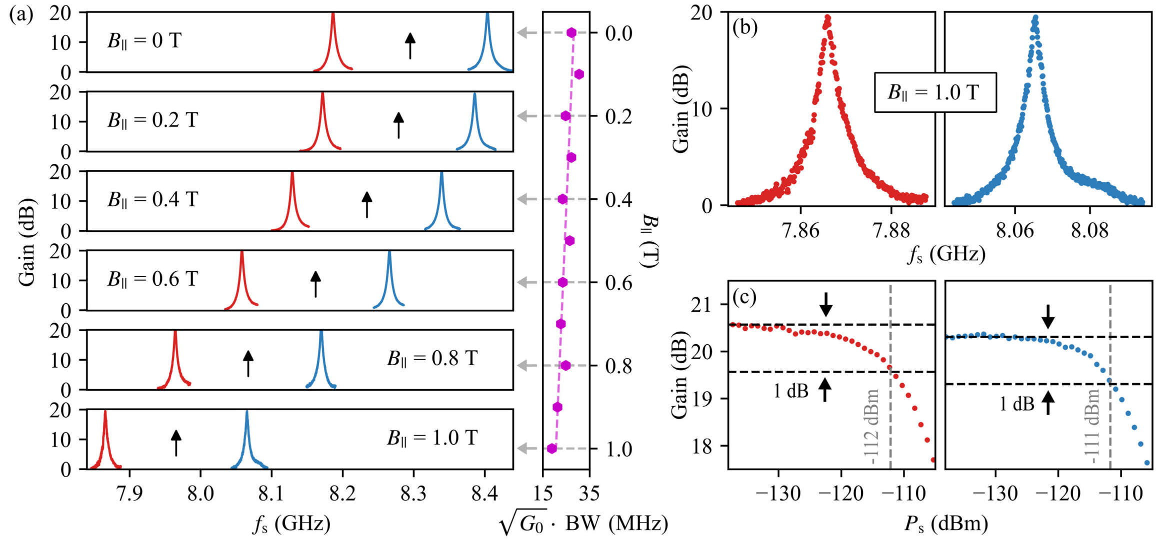

FIG. 3. Gain performance resilient to in-plane magnetic fields. (a) The six left panels show measured gain profiles at magnetic fields $B_{\parallel} = 0$, 0.2, 0.4, 0.8, and 1.0 T, applied in parallel to the grAl film. The black arrows indicate the frequency of the pump. Note that $G_0 = 20$ dB can be achieved at any field up to 1 T. The right panel depicts the gain-bandwidth product vs $B_{\parallel}$, extracted from the measured gain profiles with $G_0 = 20$ dB. The dashed purple line illustrates the $\kappa/2$ values measured from the pump off resonant response of the dimer frequencies. (b) Measured gain of the grAlPA at $B_{\parallel} = 1$ T. (c) Saturation power measurements for the two modes of the grAlPA at $B_{\parallel} = 1$ T. The 1-dB compression point is indicated by the gray labels.

We demonstrate the utility of the grAlPA in the readout of quantum devices by showing single-shot heterodyne detection of a generalized flux qubit (GFQ). The GFQ is inductively coupled to a readout resonator with linewidth $\kappa_r/2\pi = 1.25$ MHz and frequency $f_r = 8.1361$ GHz (for more details, see Ref. [79], device q8). In Fig. 4(c), we present a histogram of 8×10^5 contiguous measurements using a readout pulse of time $\tau = 0.6$ μs and power equivalent to $\bar{n}_r = 31$ circulating photons in the resonator, calibrated using the ac Stark shift of the GFQ [48]. The distribution shows two maxima corresponding to the ground $|g\rangle$ and first excited $|e\rangle$ energy states of the qubit. Using the grAlPA with $G_0 = 25$ dB, in Fig. 4(d), we plot a typical measured quantum-jump trace corresponding to an effective qubit temperature $T_q = 56$ mK. We define the quadrature $\mathrm{SNR_V}$ as the ratio between the magnitude α and

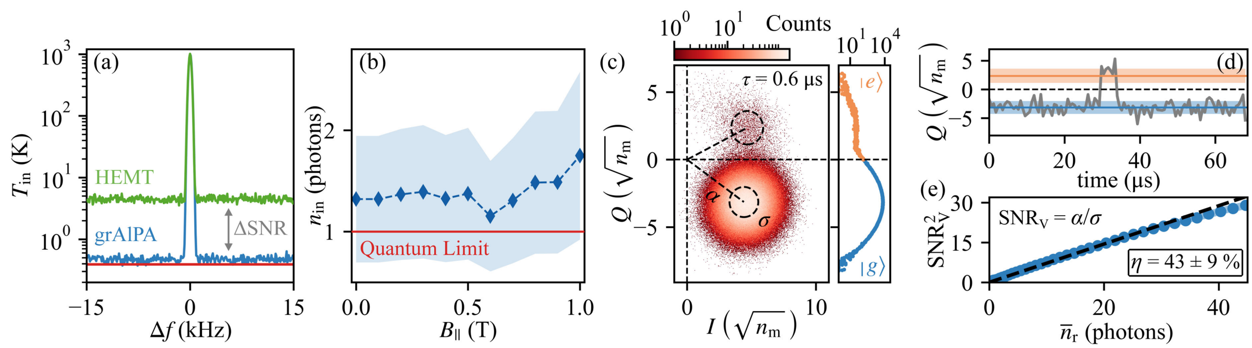

FIG. 4. Noise performance and quantum efficiency of the grAlPA. (a) Input-referred noise temperature at $B_{\parallel} = 0$ T as a function of detuning Δf from a power-calibrated tone at $f_s = 8.193$ GHz [48]. The green and blue solid lines represent measurements with the grAlPA pump off and on, respectively. When the grAlPA is on, the noise approaches the standard quantum limit for nondegenerate amplification indicated by the solid red line. The signal-to-noise improvement (ΔSNR) is defined as the ratio between the baselines of the green and blue curves. (b) Input-referred noise as a function of $B_{\parallel}$. The blue shaded area indicates the uncertainty propagated from the line-attenuation calibration. (c) Histogram of contiguous measurements of a qubit acquired using the grAlPA with $G_0 = 25$ dB. The I and Q quadratures of the readout signal are scaled in units of square root of measurements photons $\sqrt{n_m} = \sqrt{\bar{n}_r \tau \kappa_r / 4}$. The Q-axis projected histogram on the right shows measured qubit distributions corresponding to the ground $|g\rangle$ and excited $|e\rangle$ states. (d) Example of a measured quantum-jump trace. The solid lines correspond to the ground (blue) and excited (orange) states of the qubit, and the colored areas represent one standard deviation σ from the histogram in (e). (e) $\mathrm{SNR_V^2}$ as a function of readout resonator occupation $\bar{n}_r$. From a linear fit (black dashed line), we extract the readout quantum efficiency $\eta = (43 \pm 9)\%$.

standard deviation σ of the $|g\rangle$ pointer state. We fit the data using the formula $\mathrm{SNR}_\mathrm{V}^2 = \eta \bar{n}_\mathrm{r} \kappa_\mathrm{r} B^{-1}/4$, where $B^{-1} = 2/\kappa_\mathrm{r} + \tau$ is the measurement bandwidth [1,80], from which we extract a quantum efficiency $\eta = (43 \pm 9)\%$ [cf. Fig. 4(e)]. Considering the contributions of the insertion loss after the GFQ and the residual HEMT noise, we extract an intrinsic grAlPA quantum efficiency $\eta_\mathrm{gr} = 92^{+8}_{-22}\%$, corresponding to $n_\mathrm{gr} = 0.54 \pm 0.13$ added noise photons [48].

In summary, we have demonstrated a practically useful parametric amplifier, nicknamed grAlPA, which relies exclusively on granular aluminum for its nonlinearity and operates close to the quantum limit up to 1 T in-plane magnetic field. Beyond this range, spurious frequency jumps and added losses, likely resulting from residual flux trapping in the pads of the capacitors, hinder the operation of the amplifier. A potential solution is the implementation of artificial pinning sites, similar to the approach described in Refs. [77,78]. Furthermore, in order to enable enhanced frequency tunability and increased signal-pump detuning, the grAlPA concept could be expanded to three-wave mixing by using rf superconducting quantum interference device (SQUID) [69,73,81–83] made of grAl nanojunctions [62] or by applying a direct current bias [36].

Acknowledgments—We are grateful to Nicolas Roch, Patrick Winkel, and Mathieu Fechant for fruitful discussions, and we acknowledge technical support from S. Diewald and L. Radtke. Funding was provided by the Deutsche Forschungsgemeinschaft (DFG—German Research Foundation) under Project No. 450396347 (GeHoldeQED). Funding for the noise calibration was provided by the European Union under the Horizon Europe Program, Grant Agreement No. 101080152 (TruePA). I. T. and T. R. acknowledge support from the German Ministry of Education and Research (BMBF) within the project GEQCOS (FKZ: 13N15683). A. N. acknowledges financing from the Baden-Württemberg Stiftung within the Project No. QT-10 (QEDHiNet). S. Geisert and S. I. acknowledge support from the European Commission (FET-Open AVaQus GA 899561). S. Günzler, D. R., and W. W. acknowledge support from the Leibniz Award No. WE 4458-5. Facilities use was supported by the Karlsruhe Nano Micro Facility (KNMFi) and KIT Nanostructure Service Laboratory (NSL). We acknowledge qKit for providing a convenient measurement software framework.

Data availability—The data supporting the findings presented in this Letter are openly available [84].

[1] R. Vijay, D. H. Slichter, and I. Siddiqi, Observation of quantum jumps in a superconducting artificial atom, Phys. Rev. Lett. **106**, 110502 (2011).

[2] A. Roy and M. Devoret, Introduction to parametric amplification of quantum signals with Josephson circuits, C.R. Phys. **17**, 740 (2016).

[3] J. Aumentado, Superconducting parametric amplifiers: The state of the art in Josephson parametric amplifiers, IEEE Microw. Mag. **21**, 45 (2020).

[4] M. Esposito, A. Ranadive, L. Planat, and N. Roch, Perspective on traveling wave microwave parametric amplifiers, Appl. Phys. Lett. **119**, 120501 (2021).

[5] S. Krinner, N. Lacroix, A. Remm, A. Di Paolo, E. Genois, C. Leroux, C. Hellings, S. Lazar, F. Swiadek, J. Herrmann, G. J. Norris, C. K. Andersen, M. Müller, A. Blais, C. Eichler, and A. Wallraff, Realizing repeated quantum error correction in a distance-three surface code, Nature (London) **605**, 669 (2022).

[6] T. White, Readout of a quantum processor with high dynamic range Josephson parametric amplifiers, Appl. Phys. Lett. **122**, 014001 (2023).

[7] Google Quantum AI, Suppressing quantum errors by scaling a surface code logical qubit, Nature (London) **614**, 676 (2023).

[8] V. V. Sivak, A. Eickbusch, B. Royer, S. Singh, I. Tsioutsios, S. Ganjam, A. Miano, B. L. Brock, A. Z. Ding, L. Frunzio, S. M. Girvin, R. J. Schoelkopf, and M. H. Devoret, Real-time quantum error correction beyond break-even, Nature (London) **616**, 50 (2023).

[9] V. Vesterinen, O.-P. Saira, I. Räisänen, M. Möttönen, L. Grönberg, J. Pekola, and J. Hassel, Lumped-element Josephson parametric amplifier at 650 MHz for nano-calorimeter readout, Supercond. Sci. Technol. **30**, 085001 (2017).

[10] Z. K. Minev, S. O. Mundhada, S. Shankar, P. Reinhold, R. Gutiérrez-Jáuregui, R. J. Schoelkopf, M. Mirrahimi, H. J. Carmichael, and M. H. Devoret, To catch and reverse a quantum jump mid-flight, Nature (London) **570**, 200 (2019).

[11] R. Kokkoniemi, J. Govenius, V. Vesterinen, R. E. Lake, A. M. Gunyhó, K. Y. Tan, S. Simbierowicz, L. Grönberg, J. Lehtinen, M. Prunnila, J. Hassel, A. Lamminen, O.-P. Saira, and M. Möttönen, Nanobolometer with ultralow noise equivalent power, Commun. Phys. **2**, 124 (2019).

[12] Z. Wang, L. Balembois, M. Rančić, E. Billaud, M. Le Dantec, A. Ferrier, P. Goldner, S. Bertaina, T. Chanelière, D. Esteve, D. Vion, P. Bertet, and E. Flurin, Single-electron spin resonance detection by microwave photon counting, Nature (London) **619**, 276 (2023).

[13] R. Assouly, R. Dassonneville, T. Peronnin, A. Bienfait, and B. Huard, Quantum advantage in microwave quantum radar, Nat. Phys. **19**, 1418 (2023).

[14] K. W. Murch, S. J. Weber, C. Macklin, and I. Siddiqi, Observing single quantum trajectories of a superconducting quantum bit, Nature (London) **502**, 211 (2013).

[15] K. Serniak, S. Diamond, M. Hays, V. Fatemi, S. Shankar, L. Frunzio, R. J. Schoelkopf, and M. H. Devoret, Direct dispersive monitoring of charge parity in offset-charge-sensitive transmons, Phys. Rev. Appl. **12**, 014052 (2019).

[16] M. Spiecker, P. Paluch, N. Gosling, N. Drucker, S. Matityahu, D. Gusenkova, S. Günzler, D. Rieger, I. Takmakov, F. Valenti, P. Winkel, R. Gebauer, O. Sander, G. Catelani, A. Shnirman, A. V. Ustinov, W. Wernsdorfer, Y. Cohen, and I. M. Pop, Two-level system hyperpolarization using a quantum Szilard engine, Nat. Phys. **19**, 1320 (2023).

[17] M. Tinkham, *Introduction to Superconductivity* (Dover Publications, Mineola, 2004).

[18] A. Schneider, T. Wolz, M. Pfirrmann, M. Spiecker, H. Rotzinger, A. V. Ustinov, and M. Weides, Transmon qubit in a magnetic field: Evolution of coherence and transition frequency, Phys. Rev. Res. **1**, 023003 (2019).

[19] J. Krause, C. Dickel, E. Vaal, M. Vielmetter, J. Feng, R. Bounds, G. Catelani, J. M. Fink, and Y. Ando, Magnetic field resilience of three-dimensional transmons with thin-film $Al/AlO_x/Al$ Josephson junctions approaching 1 T, Phys. Rev. Appl. **17**, 034032 (2022).

[20] S. Schaal, I. Ahmed, J. A. Haigh, L. Hutin, B. Bertrand, S. Barraud, M. Vinet, C.-M. Lee, N. Stelmashenko, J. W. A. Robinson, J. Y. Qiu, S. Hacohen-Gourgy, I. Siddiqi, M. F. Gonzalez-Zalba, and J. J. L. Morton, Fast gate-based readout of silicon quantum dots using Josephson parametric amplification, Phys. Rev. Lett. **124**, 067701 (2020).

[21] V. Elhomsy, L. Planat, D. J. Niegemann, B. Cardoso-Paz, A. Badreldin, B. Klemt, V. Thiney, R. Lethiecq, E. Eyraud, M. C. Dartiailh, B. Bertrand, H. Niebojewski, C. Bäuerle, M. Vinet, T. Meunier, N. Roch, and M. Urdampilleta, Broadband parametric amplification for multiplexed SiMOS quantum dot signals, arXiv:2307.14717.

[22] M. Pita-Vidal, A. Bargerbos, R. Žitko, L. J. Splitthoff, L. Grünhaupt, J. J. Wesdorp, Y. Liu, L. P. Kouwenhoven, R. Aguado, B. van Heck, A. Kou, and C. K. Andersen, Direct manipulation of a superconducting spin qubit strongly coupled to a transmon qubit, Nat. Phys. **19**, 1110 (2023).

[23] M. Hays, V. Fatemi, D. Bouman, J. Cerrillo, S. Diamond, K. Serniak, T. Connolly, P. Krogstrup, J. Nygård, A. L. Yeyati, A. Geresdi, and M. H. Devoret, Coherent manipulation of an Andreev spin qubit, Science **373**, 430 (2021).

[24] A. Bienfait, J. J. Pla, Y. Kubo, M. Stern, X. Zhou, C. C. Lo, C. D. Weis, T. Schenkel, M. L. W. Thewalt, D. Vion, D. Esteve, B. Julsgaard, K. Mølmer, J. J. L. Morton, and P. Bertet, Reaching the quantum limit of sensitivity in electron spin resonance, Nat. Nanotechnol. **11**, 253 (2016).

[25] W. Vine, M. Savytskyi, A. Vaartjes, A. Kringhøj, D. Parker, J. Slack-Smith, T. Schenkel, K. Mølmer, J. C. McCallum, B. C. Johnson, A. Morello, and J. J. Pla, In situ amplification of spin echoes within a kinetic inductance parametric amplifier, Sci. Adv. **9**, eadg1593(2023).

[26] C. Godfrin, A. Ferhat, R. Ballou, S. Klyatskaya, M. Ruben, W. Wernsdorfer, and F. Balestro, Operating quantum states in single magnetic molecules: Implementation of Grover's quantum algorithm, Phys. Rev. Lett. **119**, 187702 (2017).

[27] S. K. Lamoreaux, K. A. van Bibber, K. W. Lehnert, and G. Carosi, Analysis of single-photon and linear amplifier detectors for microwave cavity dark matter axion searches, Phys. Rev. D **88**, 035020 (2013).

[28] K. M. Backes *et al.*, A quantum enhanced search for dark matter axions, Nature (London) **590**, 238 (2021).

[29] C. Braggio, G. Cappelli, G. Carugno, N. Crescini, R. Di Vora, M. Esposito, A. Ortolan, L. Planat, A. Ranadive, N. Roch, and G. Ruoso, A haloscope amplification chain based on a traveling wave parametric amplifier, Rev. Sci. Instrum. **93**, 094701 (2022).

[30] L. M. Janssen, G. Butseraen, J. Krause, A. Coissard, L. Planat, N. Roch, G. Catelani, Y. Ando, and C. Dickel, Magnetic-field dependence of a Josephson traveling-wave parametric amplifier and integration into a high-field setup, Phys. Rev. Appl. **22**, 054018 (2024).

[31] J. Sarkar, K. V. Salunkhe, S. Mandal, S. Ghatak, A. H. Marchawala, I. Das, K. Watanabe, T. Taniguchi, R. Vijay, and M. M. Deshmukh, Quantum-noise-limited microwave amplification using a graphene Josephson junction, Nat. Nanotechnol. **17**, 1147 (2022).

[32] G. Butseraen, A. Ranadive, N. Aparicio, K. Rafsanjani Amin, A. Juyal, M. Esposito, K. Watanabe, T. Taniguchi, N. Roch, F. Lefloch, and J. Renard, A gate-tunable graphene Josephson parametric amplifier, Nat. Nanotechnol. **17**, 1153 (2022).

[33] D. Phan, P. Falthansl-Scheinecker, U. Mishra, W. M. Strickland, D. Langone, J. Shabani, and A. P. Higginbotham, Gate-tunable superconductor-semiconductor parametric amplifier, Phys. Rev. Appl. **19**, 064032 (2023).

[34] L. J. Splitthoff, J. J. Wesdorp, M. Pita-Vidal, A. Bargerbos, Y. Liu, and C. K. Andersen, Gate-tunable kinetic inductance parametric amplifier, Phys. Rev. Appl. **21**, 014052 (2024).

[35] M. Xu, R. Cheng, Y. Wu, G. Liu, and H. X. Tang, Magnetic field-resilient quantum-limited parametric amplifier, PRX Quantum **4**, 010322 (2023).

[36] S. Frasca, C. Roy, G. Beaulieu, and P. Scarlino, Three-wave-mixing quantum-limited kinetic inductance parametric amplifier operating at 6 T near 1 K, Phys. Rev. Appl. **21**, 024011 (2024).

[37] M. Khalifa and J. Salfi, Nonlinearity and parametric amplification of superconducting nanowire resonators in magnetic field, Phys. Rev. Appl. **19**, 034024 (2023).

[38] D. J. Parker, M. Savytskyi, W. Vine, A. Laucht, T. Duty, A. Morello, A. L. Grimsmo, and J. J. Pla, Degenerate parametric amplification via three-wave mixing using kinetic inductance, Phys. Rev. Appl. **17**, 034064 (2022).

[39] A. Vaartjes, A. Kringhøj, W. Vine, T. Day, A. Morello, and J. J. Pla, Strong microwave squeezing above 1 tesla and 1 kelvin, Nat. Commun. **15**, 4229 (2024).

[40] A. Mohamed, E. Zohari, J. J. Pla, P. E. Barclay, and S. Barzanjeh, Selective single and double-mode quantum limited amplifier, Phys. Rev. Appl. **21**, 064052 (2024).

[41] N. Maleeva, L. Grünhaupt, T. Klein, F. Levy-Bertrand, O. Dupre, M. Calvo, F. Valenti, P. Winkel, F. Friedrich, W. Wernsdorfer, A. V. Ustinov, H. Rotzinger, A. Monfardini, M. V. Fistul, and I. M. Pop, Circuit quantum electrodynamics of granular aluminum resonators, Nat. Commun. **9**, 3889 (2018).

[42] K. Borisov, D. Rieger, P. Winkel, F. Henriques, F. Valenti, A. Ionita, M. Wessbecher, M. Spiecker, D. Gusenkova, I. M. Pop, and W. Wernsdorfer, Superconducting granular aluminum resonators resilient to magnetic fields up to 1 tesla, Appl. Phys. Lett. **117**, 120502 (2020).

[43] P. Winkel, K. Borisov, L. Grünhaupt, D. Rieger, M. Spiecker, F. Valenti, A. V. Ustinov, W. Wernsdorfer, and I. M. Pop, Implementation of a transmon qubit using superconducting granular aluminum, Phys. Rev. X **10**, 031032 (2020).

[44] N. Bachar, S. Lerer, S. Hacohen-Gourgy, B. Almog, and G. Deutscher, Kondo-like behavior near the metal-to-insulator

transition of nanoscale granular aluminum, Phys. Rev. B **87**, 214512 (2013).

[45] U. S. Pracht, T. Cea, N. Bachar, G. Deutscher, E. Farber, M. Dressel, M. Scheffler, C. Castellani, A. M. García-García, and L. Benfatto, Optical signatures of the superconducting Goldstone mode in granular aluminum: Experiments and theory, Phys. Rev. B **96**, 094514 (2017).

[46] F. Levy-Bertrand, T. Klein, T. Grenet, O. Dupré, A. Benoît, A. Bideaud, O. Bourrion, M. Calvo, A. Catalano, A. Gomez, J. Goupy, L. Grünhaupt, U. v. Luepke, N. Maleeva, F. Valenti, I. M. Pop, and A. Monfardini, Electrodynamics of granular aluminum from superconductor to insulator: Observation of collective superconducting modes, Phys. Rev. B **99**, 094506 (2019).

[47] F. Yang, T. Gozlinski, T. Storbeck, L. Grünhaupt, I. M. Pop, and W. Wulfhekel, Microscopic charging and in-gap states in superconducting granular aluminum, Phys. Rev. B **102**, 104502 (2020).

[48] See Supplemental Material at http://link.aps.org/supplemental/10.1103/PhysRevLett.133.260604, which includes Refs. [49–61], for additional information about the experimental methods and a detailed discussion of the power calibration.

[49] S. Probst, F. B. Song, P. A. Bushev, A. V. Ustinov, and M. Weides, Efficient and robust analysis of complex scattering data under noise in microwave resonators, Rev. Sci. Instrum. **86**, 024706 (2015).

[50] M. Janík, K. Roux, C. B. Espinosa, O. Sagi, A. Baghdadi, T. Adletzberger, S. Calcaterra, M. Botifoll, A. G. Manjón, J. Arbiol, D. Chrastina, G. Isella, I. M. Pop, and G. Katsaros, Strong charge-photon coupling in planar germanium enabled by granular aluminium superinductors, arXiv:2407.03079.

[51] G. Stan, S. B. Field, and J. M. Martinis, Critical field for complete vortex expulsion from narrow superconducting strips, Phys. Rev. Lett. **92**, 097003 (2004).

[52] O. Astafiev, A. M. Zagoskin, A. A. Abdumalikov, Jr., Yu. A. Pashkin, T. Yamamoto, K. Inomata, Y. Nakamura, and J. S. Tsai, Resonance fluorescence of a single artificial atom, Science **327**, 840 (2010).

[53] J. Y. Mutus, T. C. White, R. Barends, Y. Chen, Z. Chen, B. Chiaro, A. Dunsworth, E. Jeffrey, J. Kelly, A. Megrant, C. Neill, P. J. J. O'Malley, P. Roushan, D. Sank, A. Vainsencher, J. Wenner, K. M. Sundqvist, A. N. Cleland, and J. M. Martinis, Strong environmental coupling in a Josephson parametric amplifier, Appl. Phys. Lett. **104**, 263513 (2014).

[54] L. Grünhaupt, U. von Lüpke, D. Gusenkova, S. T. Skacel, N. Maleeva, S. Schlör, A. Bilmes, H. Rotzinger, A. V. Ustinov, M. Weides, and I. M. Pop, An argon ion beam milling process for native AlOx layers enabling coherent superconducting contacts, Appl. Phys. Lett. **111**, 072601 (2017).

[55] Technical datasheet: QCage.24 qubit chip carrier system, https://www.quantum-machines.co/products/qcage.

[56] Technical datasheet: Low noise amplifier LNF-LNC0.3-14A 1078Z, https://quantummicrowave.com/product/0-3-14-ghz-cryogenic-low-noise-amplifier.

[57] Technical datasheet: Cryogenic circulators and isolators, https://lownoisefactory.com/product/8-12-ghz-single-junction-isolator-circulator.

[58] Technical datasheet: Cryogenic directional coupler 4–12 GHz, https://quantummicrowave.com/wp-content/uploads/2020/03/QMC-CRYOCOUPLER-20-4.pdf.

[59] Technical datasheet: Non-magnetic coaxial cables with SMA connectors SC-219/50-SC, http://www.coax.co.jp/en/product/sc/219-50-sc.html.

[60] Technical datasheet: Octave-OPX+ units for heterodyne detection, https://docs.quantum-machines.co/0.1/qm-qua-sdk/docs/Hardware/octave.

[61] J. Gambetta, A. Blais, D. I. Schuster, A. Wallraff, L. Frunzio, J. Majer, M. H. Devoret, S. M. Girvin, and R. J. Schoelkopf, Qubit-photon interactions in a cavity: Measurement-induced dephasing and number splitting, Phys. Rev. A **74**, 042318 (2006).

[62] D. Rieger, S. Günzler, M. Spiecker, P. Paluch, P. Winkel, L. Hahn, J. K. Hohmann, A. Bacher, W. Wernsdorfer, and I. M. Pop, Granular aluminium nanojunction fluxonium qubit, Nat. Mater. **22**, 194 (2023).

[63] D. Rieger, S. Günzler, M. Spiecker, A. Nambisan, W. Wernsdorfer, and I. M. Pop, Fano interference in microwave resonator measurements, Phys. Rev. Appl. **20**, 014059 (2023).

[64] C. Eichler, Y. Salathe, J. Mlynek, S. Schmidt, and A. Wallraff, Quantum-limited amplification and entanglement in coupled nonlinear resonators, Phys. Rev. Lett. **113**, 110502 (2014).

[65] P. Winkel, I. Takmakov, D. Rieger, L. Planat, W. Hasch-Guichard, L. Grünhaupt, N. Maleeva, F. Foroughi, F. Henriques, K. Borisov, J. Ferrero, A. V. Ustinov, W. Wernsdorfer, N. Roch, and I. M. Pop, Nondegenerate parametric amplifiers based on dispersion-engineered Josephson-junction arrays, Phys. Rev. Appl. **13**, 024015 (2020).

[66] I. Takmakov, Minimizing the discrimination time for quantum states of an artificial atom, Ph.D. thesis, Karlsruher Institut für Technologie (KIT), 2022, 10.5445/IR/1000142961.

[67] D. Sarchi, I. Carusotto, M. Wouters, and V. Savona, Coherent dynamics and parametric instabilities of microcavity polaritons in double-well systems, Phys. Rev. B **77**, 125324 (2008).

[68] C. Eichler and A. Wallraff, Controlling the dynamic range of a Josephson parametric amplifier, Eur. Phys. J. Quantum Technol. **1**, 2 (2014).

[69] V. V. Sivak, S. Shankar, G. Liu, J. Aumentado, and M. H. Devoret, Josephson array-mode parametric amplifier, Phys. Rev. Appl. **13**, 024014 (2020).

[70] N. M. Hougland, Z. Li, R. Kaufman, B. Mesits, R. S. K. Mong, M. Hatridge, and D. Pekker, Pump-efficient Josephson parametric amplifiers with high saturation power, arXiv:2402.12586.

[71] T. Hönigl-Decrinis, R. Shaikhaidarov, S. E. de Graaf, V. N. Antonov, and O. V. Astafiev, Two-level system as a quantum sensor for absolute calibration of power, Phys. Rev. Appl. **13**, 024066 (2020).

[72] S. Günzler, P. Winkel, D. Rieger, K. Borisov, M. Spiecker, A. V. Ustinov, I. M. Pop, and W. Wernsdorfer, Superconducting microwave magnetometer for absolute flux detection, arXiv:2107.05929.

[73] N. E. Frattini, U. Vool, S. Shankar, A. Narla, K. M. Sliwa, and M. H. Devoret, 3-wave mixing Josephson dipole element, Appl. Phys. Lett. **110**, 222603 (2017).

[74] N. E. Frattini, V. V. Sivak, A. Lingenfelter, S. Shankar, and M. H. Devoret, Optimizing the nonlinearity and dissipation of a SNAIL parametric amplifier for dynamic range, Phys. Rev. Appl. **10**, 054020 (2018).

[75] R. Kaufman, T. White, M. I. Dykman, A. Iorio, G. Stirling, S. Hong, A. Opremcak, A. Bengtsson, L. Faoro, J. C. Bardin, T. Burger, R. Gasca, and O. Naaman, Josephson parametric amplifier with Chebyshev gain profile and high saturation, Phys. Rev. Appl. **20**, 054058 (2024).

[76] C. M. Caves, Quantum limits on noise in linear amplifiers, Phys. Rev. D **26**, 1817 (1982).

[77] D. Bothner, T. Gaber, M. Kemmler, D. Koelle, and R. Kleiner, Improving the performance of superconducting microwave resonators in magnetic fields, Appl. Phys. Lett. **98**, 102504 (2011).

[78] J. Kroll, F. Borsoi, K. van der Enden, W. Uilhoorn, D. de Jong, M. Quintero-Pérez, D. van Woerkom, A. Bruno, S. Plissard, D. Car, E. Bakkers, M. Cassidy, and L. Kouwenhoven, Magnetic-field-resilient superconducting coplanar-waveguide resonators for hybrid circuit quantum electrodynamics experiments, Phys. Rev. Appl. **11**, 064053 (2019).

[79] S. Geisert, S. Ihssen, P. Winkel, M. Spiecker, M. Fechant, P. Paluch, N. Gosling, N. Zapata, S. Günzler, D. Rieger, D. Bénâtre, T. Reisinger, W. Wernsdorfer, and I. M. Pop, Pure kinetic inductance coupling for cQED with flux qubits, Appl. Phys. Lett. **125**, 064002 (2024).

[80] I. Takmakov, P. Winkel, F. Foroughi, L. Planat, D. Gusenkova, M. Spiecker, D. Rieger, L. Grünhaupt, A. V. Ustinov, W. Wernsdorfer, I. M. Pop, and N. Roch, Minimizing the discrimination time for quantum states of an artificial atom, Phys. Rev. Appl. **15**, 064029 (2021).

[81] V. Sivak, N. Frattini, V. Joshi, A. Lingenfelter, S. Shankar, and M. Devoret, Kerr-free three-wave mixing in superconducting quantum circuits, Phys. Rev. Appl. **11**, 054060 (2019).

[82] A. Miano, G. Liu, V. V. Sivak, N. E. Frattini, V. R. Joshi, W. Dai, L. Frunzio, and M. H. Devoret, Frequency-tunable Kerr-free three-wave mixing with a gradiometric SNAIL, Appl. Phys. Lett. **120**, 184002 (2022).

[83] O. Naaman, D. Ferguson, A. Marakov, M. S. Khalil, W. F. Koehl, and R. J. Epstein, High saturation power Josephson parametric amplifier with GHz bandwidth, in *Proceedings of the 2019 IEEE MTT-S International Microwave Symposium (IMS)* (IEEE, New York, 2017), p. 259.

[84] N. Zapata *et al.* (2024), 10.5281/zenodo.13149677.